

Beyond Rate Coding: Surrogate Gradients Enable Spike Timing Learning in Spiking Neural Networks

Ziqiao Yu¹, Pengfei Sun¹, and Dan F. M. Goodman¹

¹*Department of Electrical and Electronic Engineering, Imperial College London*

Abstract

We investigate the extent to which Spiking Neural Networks (SNNs) trained with Surrogate Gradient Descent (Surrogate GD), with and without delay learning, can learn from precise spike timing beyond firing rates. We first design synthetic tasks isolating intra-neuron inter-spike intervals and cross-neuron synchrony under matched spike counts. On more complex spike-based speech recognition datasets (Spiking Heidelberg Digits (SHD) and Spiking Speech Commands (SSC)), we construct variants where spike count information is eliminated and only timing information remains, and show that Surrogate GD-trained SNNs are able to perform significantly above chance whereas purely rate-based models perform at chance level. We further evaluate robustness under biologically inspired perturbations – including Gaussian jitter per spike or per-neuron, and spike deletion – revealing consistent but perturbation-specific degradation. Networks show a sharp performance drop when spike sequences are reversed in time, with a larger drop in performance from SNNs trained with delays, indicating that these networks are more human-like in terms of behaviour. To facilitate further studies of temporal coding, we have released our modified SHD and SSC datasets.

1 Introduction

Spiking Neural Networks (SNNs) are biologically inspired models that compute via discrete, sparse spikes, rather than continuous activations [Maass, 1997]. This event-driven framework not only captures rich temporal patterns (such as inter-spike intervals (ISI), cross-neuron synchrony, causal spike sequences [Bohte, 2004]) but also powers energy-efficient neuromorphic hardware [Painkras et al., 2013, Akopyan et al., 2015, Davies et al., 2018, Orchard et al., 2021, Su et al., 2024].

Despite their promise, a persistent challenge remains: how to convert precise spike timing into effective learning signals. Surrogate Gradient Descent (Surrogate GD) provides a practical solution by replacing the non-differentiable spike with a smooth surrogate, thereby allowing backpropagation through time [Neftci et al., 2019]. Subsequent work has improved its efficiency and adaptiveness by enforcing sparser gradients [Perez-Nieves and Goodman, 2021] and by developing more adaptive surrogate functions [Wang et al., 2023]. Surrogate GD-trained networks have matched or outperformed rate-based RNNs on several neuromorphic benchmarks [Shrestha and Orchard, 2018, Dampfhofer and Mesquida, 2024, Hammouamri et al., 2024, Sun et al., 2025], but it remains unclear whether these successes stem from genuine temporal coding or from reliance on coarse firing-rate features.

To address this ambiguity, researchers have injected various temporal inductive biases: heterogeneous time constants [Perez-Nieves et al., 2021, Habashy et al., 2024]; learnable axonal delays [Shrestha et al., 2022, Sun et al., 2022, Patiño-Saucedo et al., 2023]; synaptic delays [Zhang et al., 2020, Yu et al., 2022, Sun et al., 2024, Hammouamri et al., 2024]; and dendritic delay models [D’agostino et al., 2024, Zheng et al., 2024]. Yet even with these enhancements, Surrogate GD alone may lack the bias needed to capture precise timing.

This uncertainty leads to a central question: *Can Surrogate GD-based SNNs learn and depend on spike timing codes beyond rate statistics?* To address this, we investigate this question through a multi-stage evaluation. First, we construct synthetic benchmark tasks that isolate the contribution of ISI and spike synchrony under controlled spike counts, building upon prior work that highlights the ability of SNNs to leverage temporal coding for classification [Bohte et al., 2002, Mirsadeghi et al., 2021]. Then, we evaluate models on datasets with real-world temporal complexity (SHD and SSC) [Cramer et al., 2020], introducing spike count-normalized variants to remove rate confounds. Finally, we assess robustness under biologically inspired perturbations—Gaussian jitter applied per-spike and per-neuron [Amarasingham et al., 2012, Agmon, 2012], spike deletions [Mainen and Sejnowski, 1995, Chen et al., 2022], and time reversal.

Our findings show that Surrogate GD-trained SNNs can extract fine-grained temporal structure even without spike rate information, including intra-neuron ISIs and cross-neuron synchrony. Delay learning further enhances the model’s ability to exploit such timing features. Across perturbations—per-spike and per-neuron Gaussian jitter, and per-spike deletion—we observe distinct degradation patterns that reveal both vulnerabilities and robustness in the model’s temporal encoding. Notably, under time reversal, Surrogate GD-trained SNNs not only leverage reversal-invariant features like ISI and coincidence, but also capture temporal dependencies in spike timing, indicating a layered temporal representation.

2 Surrogate Gradient Descent Enables Learning of Diverse Spike-Timing Codes

Throughout this section we analyse two synthetic benchmarks that isolate specific temporal features—**intra-neuron inter-spike intervals (ISI)** and **inter-neuron coincidence**. Forward propagation uses a Heaviside spike function, while back-propagation employs the smooth surrogate

$$\frac{\partial H(x)}{\partial x} \approx \frac{1}{(\alpha \cdot |x| + 1)^2}, \quad \alpha = 100, \quad (1)$$

following the general form proposed by [Nefteci et al., 2019]. Unless otherwise noted, it is used consistently across all SGD models in this work.

2.1 Surrogate GD Successfully Learns ISI-Based Temporal Codes

This experiment evaluates whether SNNs trained with surrogate gradients can learn from fine-grained inter-spike interval (ISI) structure. Each sample contains $N = 10$ input neurons, each generating spike pairs with a fixed class-specific ISI δ and firing rate r . Spikes are distributed within a $T = 1000$ ms window and placed at non-overlapping positions. The number of spikes and ISI steps are computed by:

$$\text{Number of spike pairs} = \left\lfloor r \cdot \frac{T}{1000} \right\rfloor, \quad \text{ISI steps} = \max(1, \lfloor \delta \rfloor). \quad (2)$$

The model consists of an input layer, a spiking hidden layer with 100 neurons and a shared learnable membrane time constant τ . The model is non-recurrent, and classification is based on output membrane potentials at the final time step using cross-entropy loss.

Random Replacement. To simulate timing degradation, a fraction $f \in [0, 1]$ of spikes in each neuron’s train are removed and replaced by new spikes sampled uniformly over $[0, T]$:

$$S'_i = (S_i \setminus \mathcal{R}_i) \cup \mathcal{U}_i, \quad |\mathcal{R}_i| = |\mathcal{U}_i| = \lfloor f \cdot |S_i| \rfloor. \quad (3)$$

As shown in fig. 1(c), the model achieves approximately 95% accuracy under clean input conditions ($f = 0$), successfully solving the ISI classification task. This confirms that Surrogate Gradient

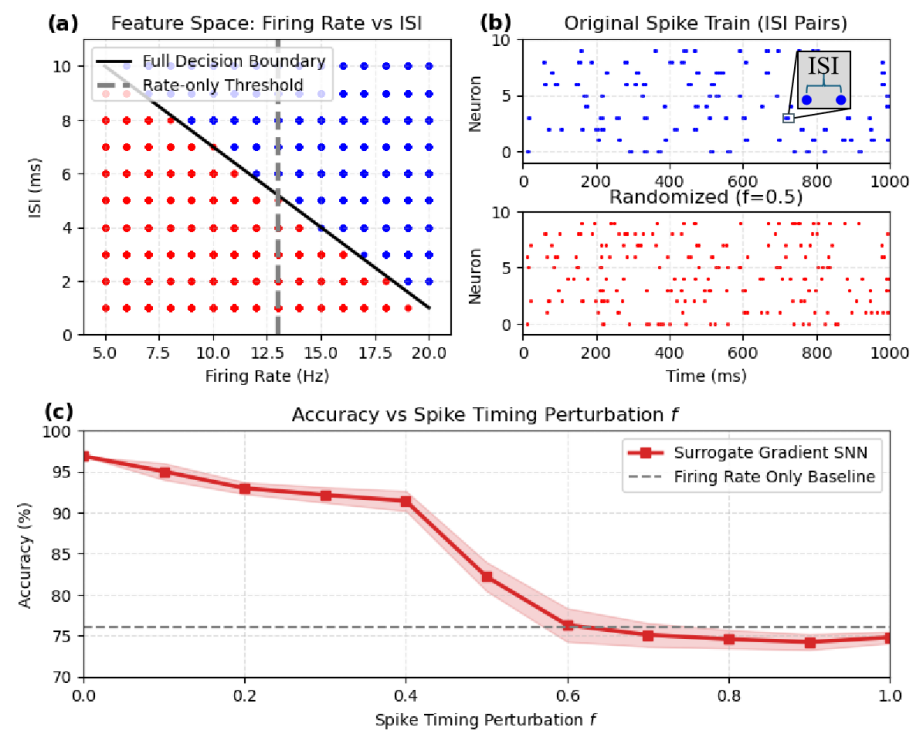


Figure 1: **ISI-based dataset.** (a) Class decision boundary in ISI-rate space. Horizontal rate-only cutoff (gray) achieves only partial separation. (b) Example spike trains generated using fixed ISI pairs (top) and their randomized counterparts with $f = 0.5$ (bottom). (c) Test accuracy under increasing spike timing perturbation f (fraction of spike times randomly redrawn). Accuracy degrades toward the spike count baseline as $f \rightarrow 1$.

Descent enables the SNN to extract information from inter-spike intervals—one of the fundamental forms of spike timing codes.

As the perturbation factor f increases, spike timing information becomes increasingly disrupted, leading to degraded model performance. For $f > 0.5$, most ISIs are broken—as each interval requires a pair of spikes—effectively eliminating temporal cues. The model then relies primarily on firing rate, with accuracy converging to approximately 75%. This is above chance level (50%) but reflects the limit of rate-based discrimination.

2.2 Surrogate GD Successfully Learns Coincidence-Based Temporal Codes

This experiment evaluates whether SNNs trained with surrogate gradient descent can classify inputs based on group-level synchrony patterns. Each sample consists of $N = 60$ input neurons evenly divided into three groups. Spikes are generated in non-overlapping windows of size $w = 10$ within a total duration T , and are restricted to a central sub-window of 5 steps to introduce mild temporal jitter while maintaining synchrony.

The class identity is defined by which two of the three groups fire synchronously while the third inverts. For example, Class A corresponds to synchrony between Groups 1 and 2, with Group 3 in OFF state. To eliminate rate-based cues, ON/OFF group activity toggles randomly in each window, and total spike count is balanced across samples.

Formally, for each window w_i , let $\mathcal{T}_i = \{t_i + 2, \dots, t_i + 6\}$ be the valid spike time slots. For each group g and class c :

$$k_i^{(g)} \sim P_c(k; \mu_{\text{on/off}}), \quad \text{activate } k_i^{(g)} \text{ neurons in group } g \text{ at times } t \in \mathcal{T}_i. \quad (4)$$

To control task difficulty, we interpolate between ON/OFF spike count distributions via a synchrony overlap factor $\lambda \in [0, 1]$:

$$\mu_{\text{on}} = (1 - \lambda) \cdot \mu_{\text{on}}^{(0)} + \lambda \cdot \mu_{\text{avg}}, \quad \mu_{\text{off}} = (1 - \lambda) \cdot \mu_{\text{off}}^{(0)} + \lambda \cdot \mu_{\text{avg}}, \quad (5)$$

where $\mu_{\text{on}}^{(0)} = 12$, $\mu_{\text{off}}^{(0)} = 2$, and $\mu_{\text{avg}} = 5$. As λ increases, the ON and OFF spike distributions converge, reducing synchrony discriminability (see fig. 2(a)).

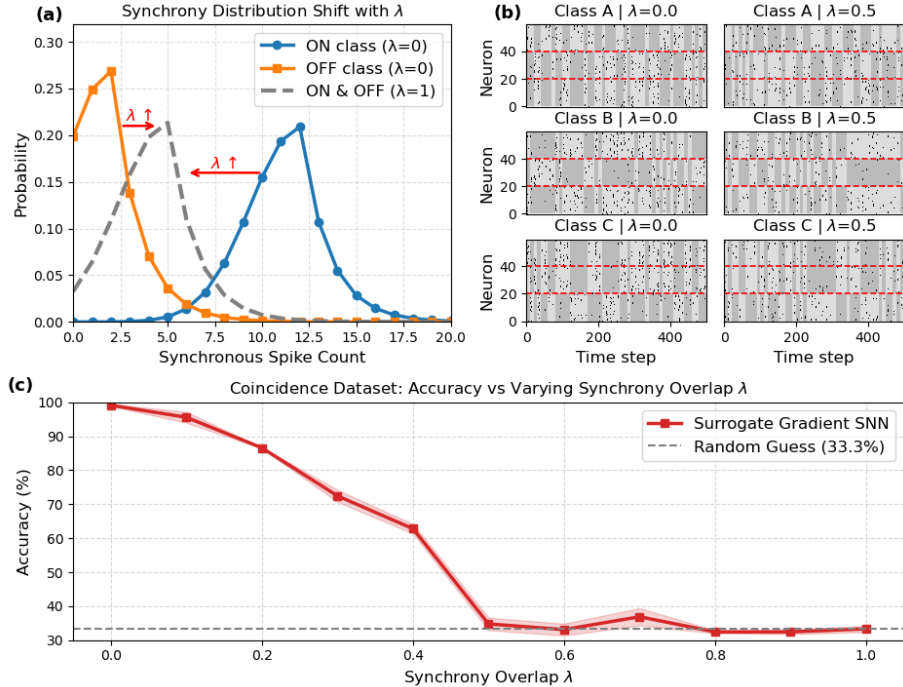


Figure 2: **Coincidence-based dataset.** (a) Synchronous spike count distributions for ON/OFF classes at $\lambda = 0$ and $\lambda = 1$. As λ increases, ON and OFF distributions converge. (b) Spike raster plots for each class under low ($\lambda = 0$) and moderate ($\lambda = 0.5$) synchrony overlap. Red lines mark group boundaries. Light gray and dark gray bands indicate ON and OFF neuron groups, respectively. (c) Test accuracy of the Surrogate GD trained SNN across varying levels of synchrony overlap λ .

We employ a compact architecture with a 60-neuron input layer, a 3-neuron spiking hidden layer (one per group), and a 3-neuron non-spiking output layer. This minimal hidden size allows direct interpretation of how synchrony patterns map to class labels. Classification is based on the final membrane potentials of the output layer using cross-entropy loss.

As shown in fig. 2(c), the model achieves near-perfect accuracy at $\lambda = 0$, indicating successful learning of group-level spike synchrony. Accuracy declines as λ increases and synchrony degrades, converging toward the rate-based baseline of 33.3%.

3 Validation of Spike Timing Learning on SHD/SSC Datasets

Motivated by our synthetic-task results showing that Surrogate GD-trained SNNs can leverage timing information, we evaluate them on more complex speech recognition datasets—SHD and SSC—which exhibit pronounced spike-count biases that allow MLPs to achieve nontrivial accuracy. To isolate genuine timing-based learning, we therefore construct two *timing-normalized* variants (see fig. 3) that remove rate information while preserving each sample’s temporal structure.

3.1 Construction of Timing-Normalized SHD and SSC Datasets

Spiking neural network (SNN) benchmarks such as SHD and SSC exhibit complex spatiotemporal spike patterns [Cramer et al., 2020]. However, their raw versions suffer from pronounced spike-count biases: some channels fire far more often than others, and overall activity levels vary significantly between classes. Consequently, even simple multilayer perceptrons trained only on per-sample spike counts can achieve nontrivial accuracy (see fig. 5), making it hard to determine whether SNNs truly leverage precise timing or simply exploit rate-based cues.

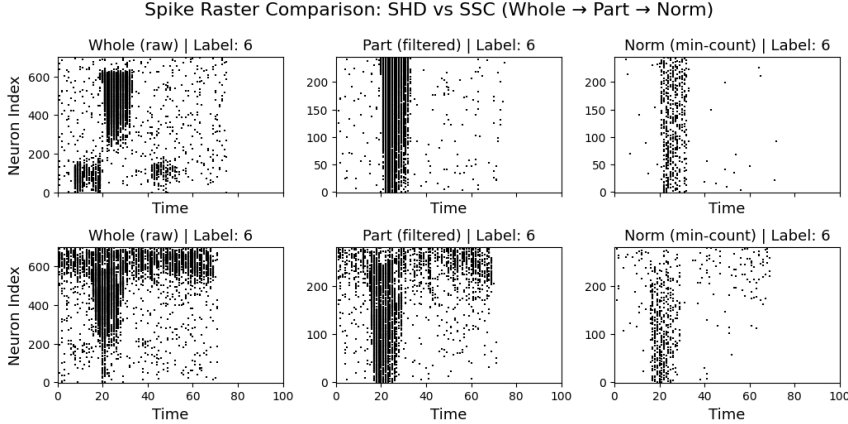


Figure 3: Example spike rasters of SHD (top) and SSC (bottom) samples across the Whole \rightarrow Part \rightarrow Norm normalization stages. Neuron selection and spike count normalization progressively remove rate-based information while retaining temporal structure.

To address this, we construct two timing-normalized variants of the SHD and SSC datasets, each with an increasing amount of rate-based information stripped away. These variants aim to eliminate spike count confounds while preserving discriminative temporal structure. The normalization process follows a two-stage strategy:

Stage 1: Neuron and Sample Filtering for Spike Count Normalization (Whole \rightarrow Part).

To eliminate rate-based information while preserving temporal structure, we aim to normalize the spike count for each neuron across all samples. However, some neurons emit zero spikes in certain samples, making exact normalization infeasible.

Let $X \in \{0, 1\}^{M \times N \times T}$ denote the dataset with M samples, N neurons, and T time steps, where $x_{m,i,t} = 1$ indicates a spike from neuron i at time t in sample m . For each neuron i , we compute its minimum spike count across samples:

$$c_i^{\min} = \min_m \sum_{t=1}^T x_{m,i,t}. \tag{6}$$

Neurons with $c_i^{\min} < \theta$ (we use $\theta = 2$) are initially marked for exclusion. However, in many cases, a neuron’s low c_i^{\min} is caused by a small number of inactive samples. To retain more neurons, we apply an additional sample filtering step: if a neuron’s low activity affects fewer than a threshold fraction of samples, we remove those samples instead of the neuron. Formally, for each neuron i , we define the set of affected samples:

$$\mathcal{M}_i = \left\{ m \mid \sum_{t=1}^T x_{m,i,t} < \theta \right\}, \tag{7}$$

and apply the condition

$$\text{if } \frac{|\mathcal{M}_i|}{M} < \epsilon, \text{ then exclude all samples in } \mathcal{M}_i. \tag{8}$$

We set $\epsilon = 0.01$ for both SHD and SSC, reflecting dataset-specific trade-offs. This introduces a balance between neuron retention and sample preservation: deleting more samples allows us to retain more neurons, but excessive deletion can skew the class distribution. To mitigate this, we avoid reducing any class below 50% of its original size. For example, in SHD, each class initially contains around 500 samples; after filtering, only Class 2 is reduced to 273 samples, while classes like Class 19 are barely affected. This strategy significantly increases neuron retention while preserving sufficient samples per class for training.

After filtering, we retain only neurons that spike at least θ times in every remaining sample, forming the **Part** variant ($N' \ll N$). To ensure a fair comparison across classes, we randomly downsample each class to match the size of the smallest one. This balancing step improves the interpretability of accuracy metrics in the subsequent experiments.

Stage 2: Min-Count Spike Normalization (Part \rightarrow Norm). To fully eliminate spike count information while preserving spike timing, we subsample each spike train to retain exactly $c_i^{\prime\min}$ spikes per neuron i in every sample, where $c_i^{\prime\min}$ is the minimum spike count across the filtered samples defined in Stage 1. Specifically, we randomly select $c_i^{\prime\min}$ spike times from each neuron’s spike train in each sample, ensuring fixed per-neuron spike counts across the dataset:

$$x_{m,i,t}^{\text{norm}} = \text{Subsample}(\{t \mid x_{m,i,t} = 1\}, c_i^{\prime\min}). \quad (9)$$

This process removes all rate-based information while retaining precise spike timing within each retained spike. However, it may distort global temporal patterns such as inter-spike intervals (ISIs) or synchrony between neurons, depending on which spikes are retained. The resulting **Norm** dataset preserves the shape of the Part variant and serves as a strict test of spike timing-based learning.

3.2 Surrogate GD Enables SNNs to Exploit Spike Timing in Real Datasets

In this work, all experiments are conducted within the SLAYER framework [Shrestha and Orchard, 2018], comparing a baseline feedforward SNN trained with surrogate gradient descent (SGD) against an enhanced variant incorporating learnable axonal delays (SGD-delay) [Sun et al., 2023].

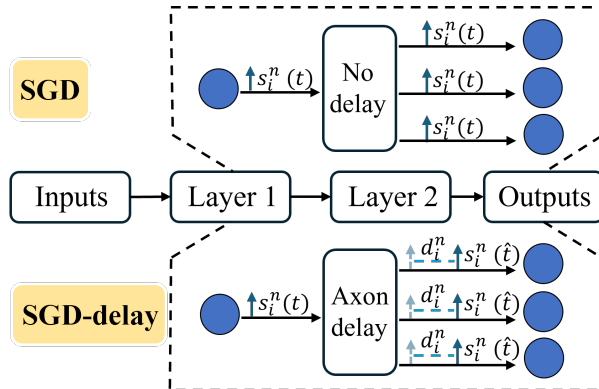


Figure 4: Comparison of SNN architectures trained with SGD and SGD-delay. The top row shows a model with no delay components. The bottom row inserts learnable axonal delays between layers.

The two architectures are illustrated in fig. 4. Both models employ a two-layer SNN, each layer comprising 128 neurons, and are trained using the Spikemax loss function [Shrestha et al., 2022]. In the SGD-delay model, axonal delays are left unbounded, allowing them to adapt freely to the data during training.

We compare SGD and SGD-delay training on the SHD and SSC datasets to evaluate their ability to extract temporal information from spike trains. Both methods are applied to three dataset variants (whole, part, norm), where the **norm** variant eliminates spike count differences across samples, isolating spike timing as the only useful cue.

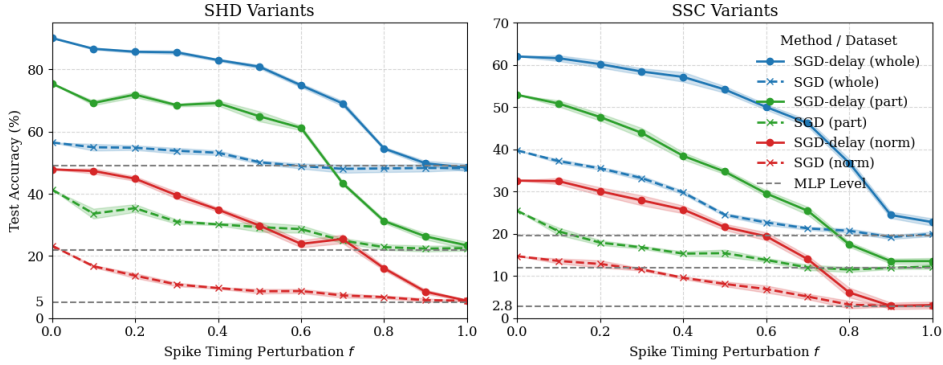


Figure 5: Test accuracy under spike timing perturbation f on SHD (left) and SSC (right) datasets. Blue: whole; green: part; red: norm. For the norm variant, spike count information is fully removed, so MLP accuracy corresponds to chance level (5% for SHD, 2.8% for SSC).

As shown in fig. 5, both SGD and SGD-delay trained SNNs outperform the MLP baseline on the norm variant (red dashed lines), demonstrating their ability to extract information from spike timing alone. This confirms that surrogate gradient based-learning is not limited to learn rate-based features but can indeed learn from precise spike timing, even without explicit delay modeling.

Notably, SGD-delay consistently achieves higher accuracy than SGD across both datasets. For instance, on SHD-norm at $f = 0$, SGD achieves 23.32% while SGD-delay reaches 47.86%; on SSC-norm, the scores are 14.69% and 32.60% respectively. These norm results serve as spike timing-only baselines and highlight the benefit of delay learning. The improvement reflects that learnable delay modules enable more accurate temporal credit assignment and introduce a stronger inductive bias toward spike timing—while incurring only minimal parameter increase: the SGD model has mn parameters, while SGD-delay adds just n additional delay terms, where m and n are the input and hidden dimensions.

Across both SHD and SSC datasets, we observe a common trend in SGD-delay’s performance: as f increases, the degradation in accuracy accelerates sharply—suggesting strong reliance on high-fidelity spike timing. Around $f=0.8$, the curves rapidly drop to the corresponding MLP baseline, after which the decay flattens out. This saturation behavior indicates that once spike timing is too corrupted to be useful, SGD-delay transitions to a rate-like regime, converging to MLP performance (chance level in the case of the norm variant).

4 SNNs Trained via Surrogate GD Are Sensitive to Temporal Structure and Reversal

4.1 Temporal Perturbations Induce Distinct but Predictable Degradation

To further evaluate the temporal sensitivity of surrogate gradient-trained SNNs, we move beyond the random spike replacement used in earlier sections (see eq. (2)), and systematically design three biologically inspired temporal distortions: Per-spike and per-neuron jitter, and per-spike deletion. These perturbations target distinct aspects of spike-based encoding and allow us to assess how each type of timing disruption affects classification performance.

(a) Per-Spike Jitter. This perturbation mimics synaptic noise by adding zero-mean Gaussian noise to individual spike times, disrupting both inter-spike intervals (ISIs) and cross-neuron synchrony while preserving spike counts:

$$t'_{i,j} = \text{clip}(t_{i,j} + \delta_{i,j}, 0, T), \quad (10)$$

where $\delta_{i,j} \sim \mathcal{N}(0, \sigma^2)$ and $\text{clip}(\cdot)$ ensures spikes remain within bounds.

(b) **Per-Neuron Jitter.** We apply a constant Gaussian time offset to all spikes emitted by a neuron, preserving intra-neuron ISI structure while disrupting precise spike-time alignment across neurons:

$$t'_{i,j} = \text{clip}(t_{i,j} + \Delta_i, 0, T), \quad (11)$$

with $\Delta_i \sim \mathcal{N}(0, \sigma_N^2)$. This perturbation tests the model’s reliance on cross-neuron synchrony for decoding.

(c) **Per-Spike Deletion.** Each spike is independently deleted with probability p_d :

$$\mathbb{P}[\text{delete } t_{i,j}] = p_d. \quad (12)$$

This distortion degrades all timing-based representations by reducing both the amount and precision of temporal cues, including ISIs, synchrony, and rate. It serves as a strong test of model robustness under severe information loss.

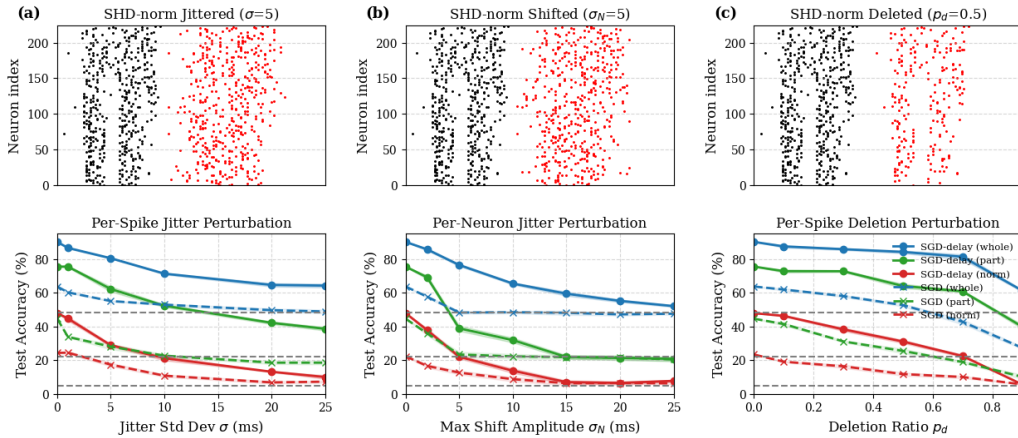


Figure 6: SNN performance under temporal perturbations: (a) Per-spike jitter, (b) per-neuron jitter, (c) per-spike deletion. **Top:** spike rasters of one specific SHD-norm sample before (black) and after (red) perturbation. **Bottom:** test accuracy across three dataset variants (Whole, Part, Norm), using SGD with and without delay learning.

We evaluate model robustness under these perturbations on all three SHD variants: whole, part, and norm (see fig. 6). First, we compare per-spike versus per-neuron jitter at high noise levels ($\sigma = \sigma_N = 25$ ms). Despite using the same Gaussian perturbation principle, the difference in granularity yields divergent results: in fig. 6(a), the model under per-spike jitter still achieves over 10% higher accuracy than the MLP baseline, whereas in fig. 6(b), per-neuron jitter degrades performance to MLP level. This suggests that per-spike jitter retains more useful temporal information. The key distinction lies in perturbation scope: per-spike jitter affects each spike individually, allowing some timing cues to survive, while per-neuron jitter shifts all spikes uniformly, eliminating relative spike timing across neurons and impairing cross-neuron synchrony more severely.

Although per-neuron jitter preserves intra-neuron ISIs by design, its performance across all dataset variants (whole, part, norm) is consistently worse than per-spike jitter, indicating that ISIs alone are not the dominant temporal feature driving classification. Instead, fine-grained inter-neuron timing appears more critical for model performance.

In contrast, fig. 6(c) shows that per-spike deletion disrupts both spike timing and count. As deletion probability increases, the performance of models trained on **whole** and **part** datasets drops below the MLP baseline, indicating that critical information—including spike redundancy and count—is lost. For the **norm** dataset, which has already been count-normalized, deletion leads to convergence near the chance level.

Overall, surrogate-trained SNNs show consistent degradation trends under timing perturbations, but their vulnerability depends strongly on the type of distortion. Fine-grained jitter preserves more

information than coarse neuron-level shifts, while deletion, by directly removing spikes, proves the most destructive.

4.2 Vulnerable to Time Reversal Like Humans

Humans are highly sensitive to the causal structure of sensory input—e.g., speech played backward becomes unintelligible [Saberi and Perrott, 1999]. To examine whether SNNs exhibit similar temporal sensitivity, we conduct a **time reversal** experiment by reversing spike trains within their active time windows.

Given an input $x \in \{0, 1\}^{N \times T}$, we identify the minimal interval containing all spikes:

$$[t_{\text{start}}, t_{\text{end}}] = [\min\{t \mid x_{i,t} = 1\}, \max\{t \mid x_{i,t} = 1\}], \quad (13)$$

and reverse each neuron’s spike sequence within this interval:

$$x'_{i,t} = x_{i,t_{\text{start}}+t_{\text{end}}-t}, \quad \forall t \in [t_{\text{start}}, t_{\text{end}}], \quad (14)$$

preserving spike count and neuron identity, but inverting the temporal order.

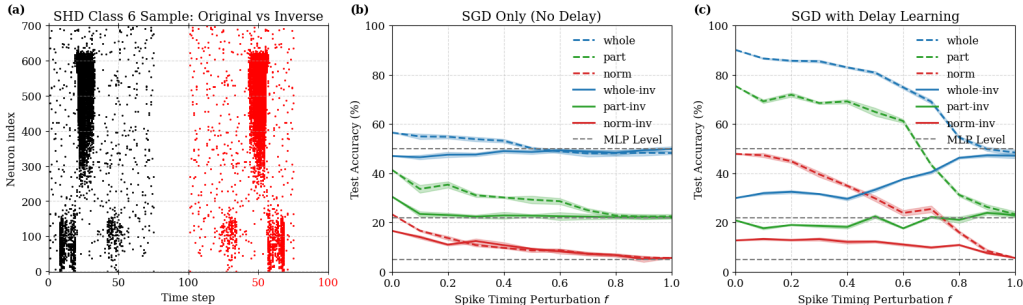


Figure 7: Test accuracy under spike timing perturbation f for original and time-reversed SHD variants. (a) Spike raster of a single sample before and after temporal inversion. (b) Results for models trained with SGD. (c) Results for models trained with SGD-delay. Each curve corresponds to one of the **whole**, **part**, or **norm** datasets in both original and inverted forms.

We evaluate pretrained surrogate gradient models on time-reversed SHD variants to assess their sensitivity to reversed temporal structure. Without retraining, we test zero-shot generalization to time-inverted inputs by applying the transformation in eq. (14). Additionally, we introduce varying levels of random perturbation f to examine whether noise can mitigate the impact of reversal.

Figure 7 reveals both reversal-induced vulnerability and reversal-invariant robustness in surrogate-trained SNNs. For the **whole-inv** dataset, accuracy is lowest at $f=0$ in both fig. 7(b) and (c), where precise yet reversed spike timing strongly misleads the model—especially for SGD-delay, which learns richer temporal dependencies. As f increases and spike timings become progressively randomized, this misleading structure is weakened, and accuracy gradually recovers. This suggests that temporal noise suppresses harmful patterns and shifts the model’s reliance from spike timing to spike count.

In contrast, for the **norm-inv** datasets, the SGD-trained SNNs in both panels achieve accuracy above the MLP baseline at $f = 0$. This suggests that SGD enables the models to learn spike timing features—such as inter-spike intervals (ISIs) or cross-neuron synchrony—that remain informative even when the temporal order of the input is reversed.

Interestingly, for both the SGD and SGD-delay trained models, the inverse variants exhibit a progressive trend relative to the MLP baseline: **whole-inv** performs below MLP level, **part-inv** remains close to MLP, and **norm-inv** achieves above-MLP accuracy. This monotonic shift suggests that the **whole** dataset contains a substantial amount of spike timing information that is sensitive to time reversal, which misleads the models when temporal order is inverted. As we move from

whole to **part** then to **norm**, many of these vulnerable temporal features are progressively filtered out by construction.

These findings demonstrate that SNNs trained via surrogate gradient descent exhibit human-like sensitivity to temporal causality: they perform well when the input follows natural time order but misfire under reversal—mirroring the well-known phenomenon that time-reversed sensory inputs (e.g., speech) are often unintelligible to humans.

5 Discussion

Surrogate gradient descent and related methods [Neftci et al., 2019, Shrestha and Orchard, 2018] have proven themselves exceptionally capable at the challenging task of training non-differentiable spiking neural networks to carry out challenging tasks. However, the question remains whether or not the solutions found using these algorithms cover the full range of capabilities of spiking neural networks, or whether they are biased to a particular subfamily of solutions. In both cases, are the solutions found similar to what biological neural networks would learn? We addressed the particular question of the extent to which timing rather than rate of action potentials can be used.

In principle, a timing-based code can be vastly more efficient than a rate-based one. Suppose spike times were accurate to within 1 ms and there was no restriction on firing rate, then for a k ms window, spike count can encode $k + 1$ different values whereas with spike timing we can encode 2^k values. In practice, the presence of neural noise and the difficulty of decoding the full range of possible timing codes will limit this. Some of the aspects of spike timing that certainly are robustly decodable include: inter-spike intervals (the time between spikes), cross-neuron coincidences, and at least some more complex spatio-temporal spike patterns. In our results, we have shown that surrogate gradient descent-based methods are able to extract information using all of these aspects of timing-based codes, in both controlled synthetic datasets and messier datasets based on recorded speech. In addition, under various forms of spike time perturbation they degrade gracefully in the majority of cases.

In particular, we looked at the Spiking Heidelberg Digits and Spiking Speech Commands datasets (SHD, SSC). These have become widely used benchmarks in the field of spiking neural networks and neuromorphic computing. We find that these datasets do contain substantial and exploitable temporal information, but that it is also possible to perform surprisingly accurate classification using spike counts only, or following various types of perturbation of the spike timing. As a consequence, this dataset may not be ideal if we wish to probe the extent to which various spike-based models can exploit temporal information. We built a derived dataset (SHD-norm) which, by construction, eliminates all spike count information. (Note that although the only information remaining in this dataset is temporal, it is likely that a significant amount of temporal information is also removed by the transformations applied.) We have made a public release of this dataset to facilitate further research on timing-based computation in spiking neural networks.

Finally, we address the question of whether or not these algorithms find solutions that are biologically feasible by considering what happens when you train a network on a set of sounds, and then test it by reversing those sounds. Since humans perform badly at this task, we would expect models that learn in a way that is more similar to humans to also perform badly. We find that spiking neural networks both with and without delays are negatively impacted by time reversal, but that networks with delays are much more significantly impacted. This suggests that networks with delays may be more biologically relevant, at least in the case of modeling the auditory system, where we know that timing information is important.

In future work, it would be interesting to investigate other aspects of spike timing-based codes, for example temporal order (A fires before B), or a more fine-grained analysis of which spatio-temporal spike patterns can be learned. It would also be interesting to devise further datasets of real-world complexity in which temporal information is substantially more important than rate-based information.

Data and Code

All code is available at the GitHub repository: <https://github.com/neural-reckoning/temporal-shd>.
The datasets are archived on Zenodo[Yu et al., 2025] (<https://doi.org/10.5281/zenodo.16153275>).

Acknowledgements

This project is partly funded by the Advanced Research + Invention Agency (ARIA).

References

- Wolfgang Maass. Networks of spiking neurons: the third generation of neural network models. *Neural networks*, 10(9):1659–1671, 1997.
- Sander M Bohte. The evidence for neural information processing with precise spike-times: A survey. *Natural Computing*, 3(2):195–206, 2004.
- Eustace Painkras, Luis A Plana, Jim Garside, Steve Temple, Francesco Galluppi, Cameron Patterson, David R Lester, Andrew D Brown, and Steve B Furber. Spinnaker: A 1-w 18-core system-on-chip for massively-parallel neural network simulation. *IEEE Journal of Solid-State Circuits*, 48(8):1943–1953, 2013.
- Filipp Akopyan, Jun Sawada, Andrew Cassidy, Rodrigo Alvarez-Icaza, John Arthur, Paul Merolla, Nabil Imam, Yutaka Nakamura, Pallab Datta, Gi-Joon Nam, et al. Truenorth: Design and tool flow of a 65 mw 1 million neuron programmable neurosynaptic chip. *IEEE transactions on computer-aided design of integrated circuits and systems*, 34(10):1537–1557, 2015.
- Mike Davies, Narayan Srinivasa, Tsung-Han Lin, Gautham China, Yongqiang Cao, Sri Harsha Choday, Georgios Dimou, Prasad Joshi, Nabil Imam, Shweta Jain, et al. Loihi: A neuromorphic manycore processor with on-chip learning. *Ieee Micro*, 38(1):82–99, 2018.
- Garrick Orchard, E Paxon Frady, Daniel Ben Dayan Rubin, Sophia Sanborn, Sumit Bam Shrestha, Friedrich T Sommer, and Mike Davies. Efficient neuromorphic signal processing with loihi 2. In *2021 IEEE Workshop on Signal Processing Systems (SiPS)*, pages 254–259. IEEE, 2021.
- Zhe Su, Simone Ramini, Demetra Coffen Marcolin, Alessandro Veronesi, Milos Krstic, Giacomo Indiveri, Davide Bertozzi, and Steven M Nowick. An ultra-low cost and multicast-enabled asynchronous noc for neuromorphic edge computing. *IEEE Journal on Emerging and Selected Topics in Circuits and Systems*, 2024.
- Emre O Neftci, Hesham Mostafa, and Friedemann Zenke. Surrogate gradient learning in spiking neural networks: Bringing the power of gradient-based optimization to spiking neural networks. *IEEE Signal Processing Magazine*, 36(6):51–63, 2019.
- Nicolas Perez-Nieves and Dan Goodman. Sparse spiking gradient descent. *Advances in Neural Information Processing Systems*, 34:11795–11808, 2021.
- Ziming Wang, Runhao Jiang, Shuang Lian, Rui Yan, and Huajin Tang. Adaptive smoothing gradient learning for spiking neural networks. In *International conference on machine learning*, pages 35798–35816. PMLR, 2023.
- Sumit B Shrestha and Garrick Orchard. Slayer: Spike layer error reassignment in time. *Advances in neural information processing systems*, 31, 2018.
- Manon Dampfhofer and Thomas Mesquida. Neuromorphic lip-reading with signed spiking gated recurrent units. In *Proceedings of the IEEE/CVF Conference on Computer Vision and Pattern Recognition*, pages 2141–2151, 2024.

- Ilyass Hammouamri, Ismail Khalfaoui Hassani, and Timothée Masquelier. Learning delays in spiking neural networks using dilated convolutions with learnable spacings. In *ICLR*, 2024.
- Pengfei Sun, Jibin Wu, Paul Devos, and Dick Botteldooren. Towards parameter-free attentional spiking neural networks. *Neural Networks*, 185:107154, 2025.
- Nicolas Perez-Nieves, Vincent CH Leung, Pier Luigi Dragotti, and Dan FM Goodman. Neural heterogeneity promotes robust learning. *Nature communications*, 12(1):5791, 2021.
- Karim G Habashy, Benjamin D Evans, Dan FM Goodman, and Jeffrey S Bowers. Adapting to time: Why nature may have evolved a diverse set of neurons. *PLOS Computational Biology*, 20(12): e1012673, 2024.
- Sumit Bam Shrestha, Longwei Zhu, and Pengfei Sun. Spikemax: spike-based loss methods for classification. In *2022 international joint conference on neural networks (IJCNN)*, pages 1–7. IEEE, 2022.
- Pengfei Sun, Longwei Zhu, and Dick Botteldooren. Axonal delay as a short-term memory for feed forward deep spiking neural networks. In *ICASSP 2022-2022 IEEE international conference on acoustics, speech and signal processing (ICASSP)*, pages 8932–8936. IEEE, 2022.
- Alberto Patiño-Saucedo, Amirreza Yousefzadeh, Guangzhi Tang, Federico Corradi, Bernabé Linares-Barranco, and Manolis Sifalakis. Empirical study on the efficiency of spiking neural networks with axonal delays, and algorithm-hardware benchmarking. In *2023 IEEE International Symposium on Circuits and Systems (ISCAS)*, pages 1–5, 2023. doi:[10.1109/ISCAS46773.2023.10181778](https://doi.org/10.1109/ISCAS46773.2023.10181778).
- Malu Zhang, Jibin Wu, Ammar Belatreche, Zihan Pan, Xiurui Xie, Yansong Chua, Guoqi Li, Hong Qu, and Haizhou Li. Supervised learning in spiking neural networks with synaptic delay-weight plasticity. *Neurocomputing*, 409:103–118, 2020.
- Qiang Yu, Jialu Gao, Jianguo Wei, Jing Li, Kay Chen Tan, and Tiejun Huang. Improving multispikes learning with plastic synaptic delays. *IEEE Transactions on Neural Networks and Learning Systems*, 34(12):10254–10265, 2022.
- Pengfei Sun, Jibin Wu, Malu Zhang, Paul Devos, and Dick Botteldooren. Delay learning based on temporal coding in spiking neural networks. *Neural Networks*, 180:106678, 2024.
- Simone D’agostino, Filippo Moro, Tristan Torchet, Yiğit Demirağ, Laurent Grenouillet, Niccolò Castellani, Giacomo Indiveri, Elisa Vianello, and Melika Payvand. Denram: neuromorphic dendritic architecture with rram for efficient temporal processing with delays. *Nature communications*, 15(1):3446, 2024.
- Hanle Zheng, Zhong Zheng, Rui Hu, Bo Xiao, Yujie Wu, Fangwen Yu, Xue Liu, Guoqi Li, and Lei Deng. Temporal dendritic heterogeneity incorporated with spiking neural networks for learning multi-timescale dynamics. *Nature Communications*, 15(1):277, 2024.
- Sander M Bohte, Joost N Kok, and Han La Poutre. Error-backpropagation in temporally encoded networks of spiking neurons. *Neurocomputing*, 48(1-4):17–37, 2002.
- Maryam Mirsadeghi, Majid Shalchian, Saeed Reza Kheradpisheh, and Timothée Masquelier. Stidi-bp: Spike time displacement based error backpropagation in multilayer spiking neural networks. *Neurocomputing*, 427:131–140, 2021.
- Benjamin Cramer, Yannik Stradmann, Johannes Schemmel, and Friedemann Zenke. The heidelberg spiking data sets for the systematic evaluation of spiking neural networks. *IEEE Transactions on Neural Networks and Learning Systems*, 33(7):2744–2757, 2020.
- Asohan Amarasingham, Matthew T Harrison, Nicholas G Hatsopoulos, and Stuart Geman. Conditional modeling and the jitter method of spike resampling. *Journal of neurophysiology*, 107(2): 517–531, 2012.

- Ariel Agmon. A novel, jitter-based method for detecting and measuring spike synchrony and quantifying temporal firing precision. *Neural systems & circuits*, 2(1):5, 2012.
- Zachary F Mainen and Terrence J Sejnowski. Reliability of spike timing in neocortical neurons. *Science*, 268(5216):1503–1506, 1995.
- Junren Chen, Chenxi Wu, Giacomo Indiveri, and Melika Payvand. Reliability analysis of memristor crossbar routers: collisions and on/off ratio requirement. In *2022 29th IEEE International Conference on Electronics, Circuits and Systems (ICECS)*, pages 1–4. IEEE, 2022.
- Pengfei Sun, Yansong Chua, Paul Devos, and Dick Botteldooren. Learnable axonal delay in spiking neural networks improves spoken word recognition. *Frontiers in Neuroscience*, 17:1275944, 2023.
- Kouros Saberi and David R Perrott. Cognitive restoration of reversed speech. *Nature*, 398(6730):760–760, 1999.
- Ziqiao Yu, Pengfei Sun, and Dan Goodman. Temporal-shd, July 2025. URL <https://doi.org/10.5281/zenodo.16153275>.